Electronic Supplementary Information (ESI):

A. Neutron reflectivity data analysis

The $\log_{10}R(q)$ profiles were obtained by a pre-treatment of the raw data from the 2-D detector. The time-of-flight detector image shows the number of neutrons reflected at a given reflection angle with respect to the wavelength. The reflectivity is the number of neutrons in the specular reflection, where the reflection angle equals the incident angle, divided by the number of incident neutrons on the sample for discrete narrow bands of wavelengths. This treatment was performed using the standard data reduction software COSMOS, a routine provided by the Instiut Laue-Langevin (ILL, Grenoble, France) in the framework of LAMP.[1] The data were normalized relative to the total reflection of an air–D_2O sample below the critical edge.

For this work it was very important to optimize the background treatment of the data since very low reflectivity values were recorded at the end of the oxidation reaction of *d*-methyl oleate (*d*-MO) and one of our aims was to quantify these very small surface excesses. To address this point, we carried out systematic investigations on several acquisitions of a clean air–air-contrast matched water (ACMW) interface where the surface excess is zero and the fitted surface excess of a hypothetical monolayer should also be zero. These tests highlighted two important problems with the background subtraction method for our application. First, the background given by an air–ACMW interface shows a characteristic shape (and curvature) with respect to the reflection angle due to the instrument/sample geometry and incoherent scattering of H-atoms.[2] The background subtraction procedure with COSMOS consists of subtracting the average of the number of neutrons with respect to the wavelength over an interval of pixels on one or both sides of the specular peak from the number of neutrons in the defined specular peak. This approach is imperfect when the reflectivity is low compared with the background. Second, even with perfect background subtraction, an equal distribution of negative and positive points around zero would result. In this case, standard data treatment would ignore the negative points,[3] and the positive points would result in a surface excess which is weighted positively. As a result of these problems, we adopted an alternative approach of not subtracting the background from the data and instead including it as a parameter in the applied model to fit the $\log_{10}R(q)$ profiles. The residual surface excess attributed to a clean air–ACMW surface was then minimized to $< 0.1\%$ monolayer coverage as opposed to $> 2\%$ monolayer coverage when the background was subtracted. As a result our ability to quantify the surface excess at the end of the oxidation reactions was improved greatly.

The fitting routine used is Motofit which runs in IgorPro.[4] The program allows one to build an optical matrix model to simulate the reflectivity of a given interfacial structure or fit parameters using a weighted least-squares fitting procedure which affects the reflectivity of experimental data. The model used is made up by semi-infinite extended ambient-phase (air) and sub-phase (ACMW), and between them there is a single deuterated monolayer. The layer was described by a homogeneous scattering length density and a thickness. The roughness values of the air–monolayer and monolayer–sub-phase interfaces and the background value were additional parameters. The roughness values were both approximated to 3 Å to be consistent with capillary wave theory given that the surface tension was always > 65 mN m^{-1}. A contribution for the inter-mixing of the reactant with possible products of limited duration in the monolayer is ignored on the basis that at the very low Q values measured the effect of small changes to the roughness value used has a negligible effect on the fitted surface excess.

The following procedure was used so that a single value of the background (*i.e.* linear with respect to *q*) could be incorporated into the model. The value of the background was refined by a systematic variation of the value to fit a hypothetical monolayer at the clean air–ACMW interface: when the chosen background value was too low a positive surface excess was fitted, and when it was correct or too high the value tended to zero. The background value was refined as 3.4×10^{-5}; see Fig. S1.

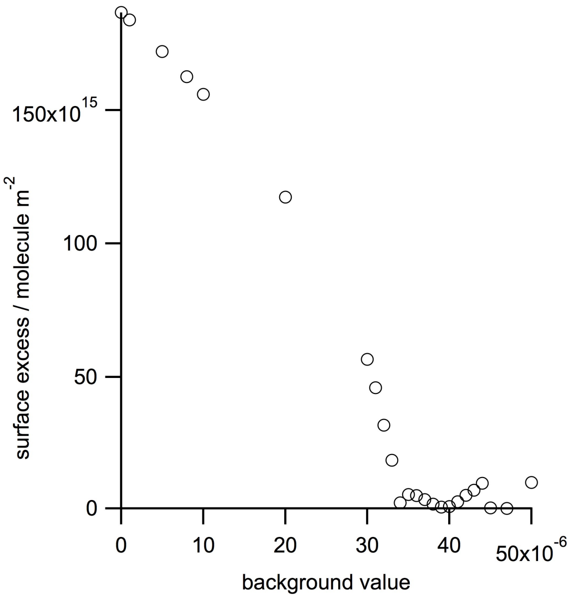

Figure S1. Optimization of the background values obtained by fitting $\log_{10}R(q)$ profiles recorded on a clear air–ACMW interface.

As the fitted surface excess of a clean air–ACMW interface was < 0.1% of a monolayer using the minimum background level possible with this approach, it was not necessary to adopt further corrections to account for the non-linear contribution to the background with respect to *q*, as any additional specular reflectivity in the kinetic measurements must have arisen from surface active material. The contribution to the specular reflectivity from uncertainties in the composition of the ACMW sub-phase was neglected because a precision balance to 0.01 g was used to make 1 kg of the sub-phase on each occasion.

Our next decision concerned whether to fit the thickness (*d*) or the scattering length density (ρ) (or both) of the monolayer during the oxidation reaction. A model that is physically realistic for an organic monolayer both at high and low coverage would be the ideal case: a disadvantage of fixing the thickness is that in reality a disordered monolayer such as deuterated methyl oleate, *d*-MO, does not have the same thickness at low and high coverage as the chains are in the fluid phase; a disadvantage of fixing the scattering length density is that we need to quantify the surface excess precisely at very low coverage where the molecules lie down and hence the thickness does not converge to zero. The optimal approach to adopt was investigated by carrying out tests on data from a monolayer of *d*-MO that was exposed to O_3. The maximum value of the thickness was provided by the fitting of a reflectivity profile of a full *d*-MO monolayer recorded over a broader *q*-range, i.e. up to 0.25 $Å^{-1}$ using neutrons with incident angles of 0.62 and 3.8°. The fitted value of the thickness was (21 ± 1) Å (see Fig. S2 (a) for the reflectivity profile together with the fitted line resulting in the quoted layer thickness). Fig. S2 (b) shows how three fitting approaches for reflectivity profiles affect the resulting surface excess profile of a full monolayer during the oxidation: (a) fixed *d* and fitted ρ, (b) fitted *d* and fixed ρ, (c) fitted *d* and fixed ρ if *d* is bigger than 4 Å and otherwise *d* = 4 Å and fitted ρ (the value 4 Å was chosen based on an estimate of the minimum thickness that a surfactant monolayer can reach when the molecules have the tails parallel to the interface). The three approaches gave the same results within the error bars (an uncertainty of < 1% monolayer coverage), so we decided to analyze all the data fixing the thickness of the layer and fitting the scattering length density. Table S1 summarizes the chosen parameters.

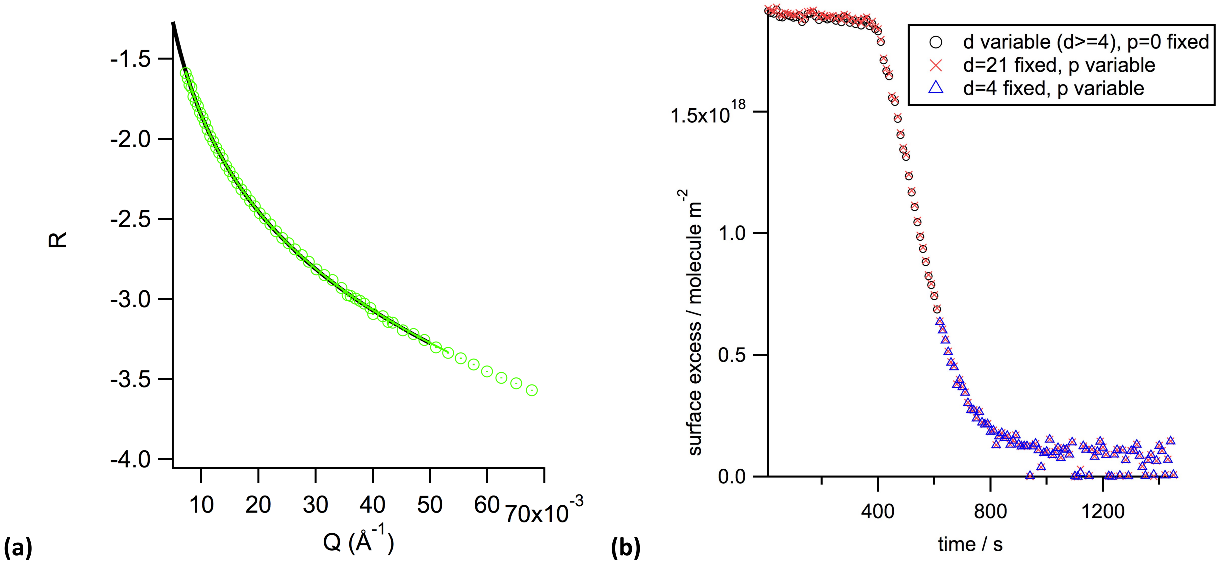

Figure S2. **(a)** Neutron reflectivity, *R*, as a function of momentum transfer, *Q*. The depicted fit (black line) results in a layer thickness of 2.1 nm; **(b)** The three fitting approaches described above lead to negligible uncertainties; the error bars are omitted for clarity.

Table S1. List of parameters used for the fitting of the reflectivity profile.

background value	3.4×10^{-5}
ρ ambient phase (air)	0 Å^{-2}
ρ sub-phase (ACMW)	0 Å^{-2}
thickness monolayer	21 Å
roughness air–monolayer	3 Å
roughness ACMW–monolayer	3 Å

The surface excess reproducibly decays to a final coverage of 6.9% at long reaction times and is stable for several hours. A test was done to re-compress this residual sparse film and continue its exposure to ozone to see if the reorientation of *d*-MO at low surface coverage simply rendered the active oxidation site inaccessible; see Fig. S3. No significant further loss of material was observed, which led us to conclude that this residual film was either an insoluble, involatile reaction product or an unreactive, insoluble, involatile deuterated impurity in the original batch of *d*-MO.

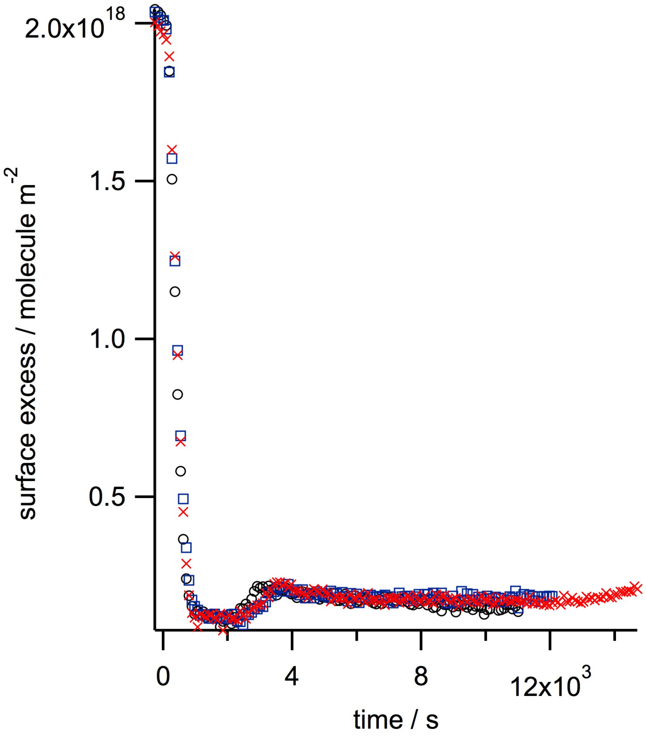

Figure S3. Oxidation of a *d*-MO monolayer by ozone followed by recompression and further exposure of the monolayer to ozone; repeats were carried out and runs are shown in different colours.

The entire study was carried out on the same batch of *d*-MO, yet decays of a freshly synthesized batch of *d*-MO showed that the final coverage was 1.8% – see example in Fig. S4; note that the contribution to the surface excess from the counting statistics of 300 s co-added data was < 0.1% as determined from the same analysis approach on air–ACMW data. The difference in these signals was therefore attributed to a 5% unreactive, insoluble, involatile deuterated impurity in the original batch of *d*-MO.

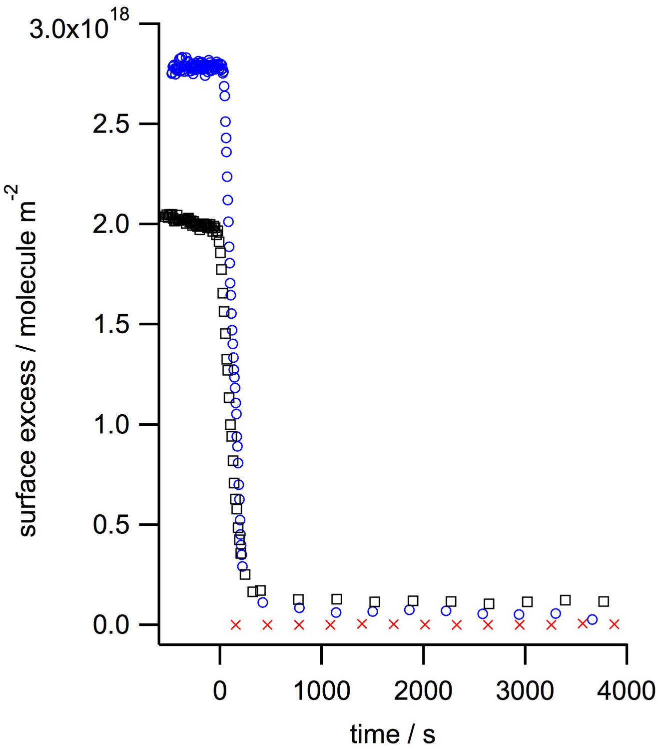

Figure S4. Oxidative decay of *d*-MO used in this study (black squares) and a new highly pure batch (blue circles); ACMW data shown for references (red crosses).

Neutron beam time is sufficiently expensive with long delays to acquire that it was decided not to repeat the entire experiment with the fresh batch of *d*-MO. Instead 5% coverage was subtracted from the surface excess data before the kinetic analysis. The loss of surface-active material resulting from the reaction of *d*-MO with ozone was therefore concluded to be > 98%.

B. Individual fits to experimental data

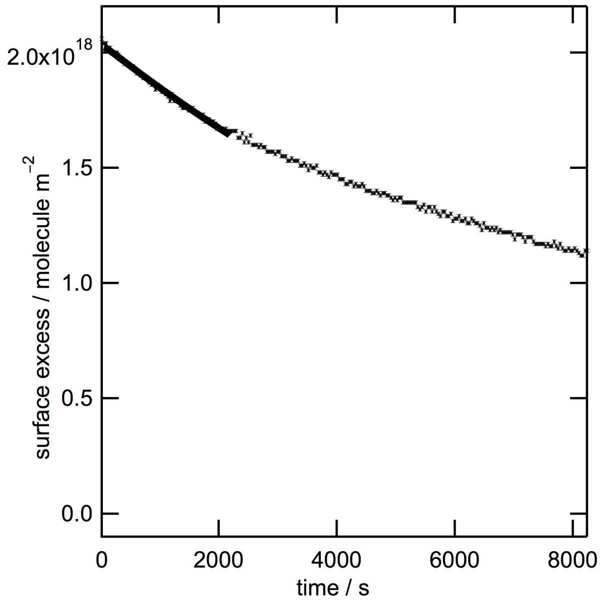

Figure S5. Surface excess of a monolayer of *d*-MO in presence of O_2 *vs*. time ('blank'). The slow loss in absence of ozone may be caused by a range of factors including loss of the organic surfactant e.g. underneath the trough's barriers, slow removal e.g. by oxygen or minor mechanical vibrations introduced by the relatively high gas flow rate (15 L min^{-1}). The fitted line provides an upper limit for this non-reactive decay (see run 12 in Table 1 of the main manuscript).

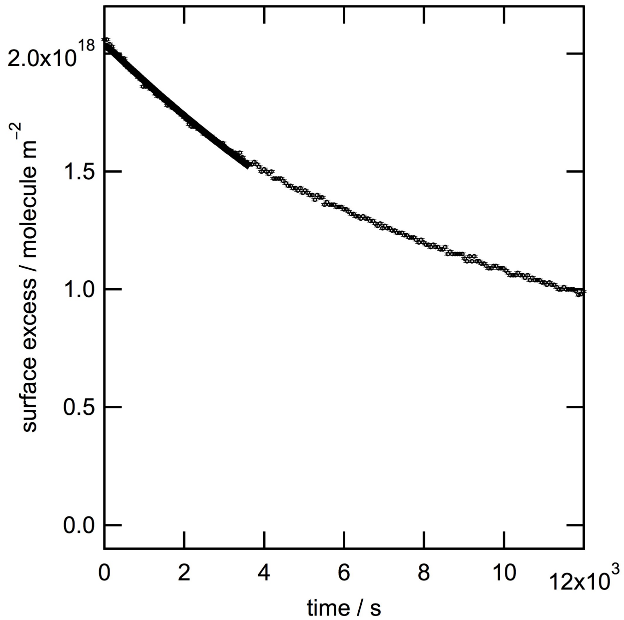

Figure S6. Surface excess of a monolayer of *d*-MO in presence of O_2 *vs*. time (repeat of 'blank' experiment presented in Fig. S5). The fitted line provides an upper limit for this non-reactive decay (see run 13 in Table 1 of the main manuscript).

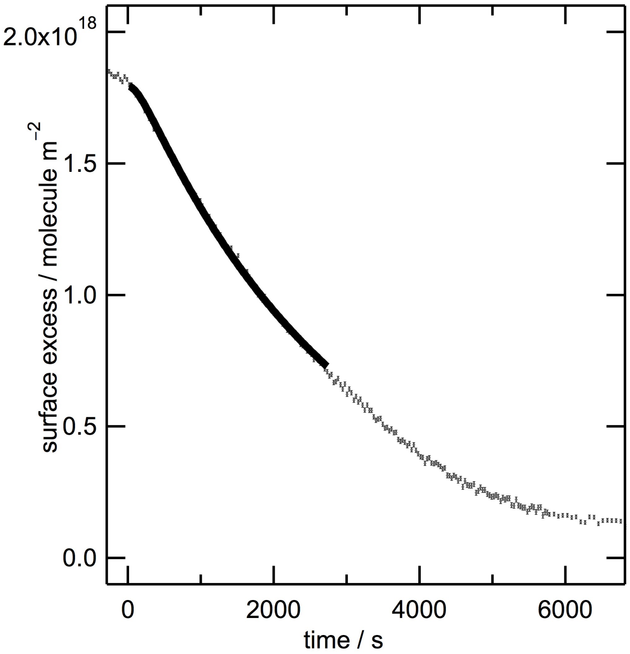

Figure S7. Surface excess of the ozonolysis of a monolayer of *d*-MO *vs*. time. *In situ* O_3-generation was initiated at $t = 0$. The solid line is a fit considering reactive decay and initial build-up of $[O_3]$ for $[O_3]_{in}$ = 7 ppb using fast-flow conditions to limit the effects of gas mixing (see run 1 in Table 1 of the main manuscript).

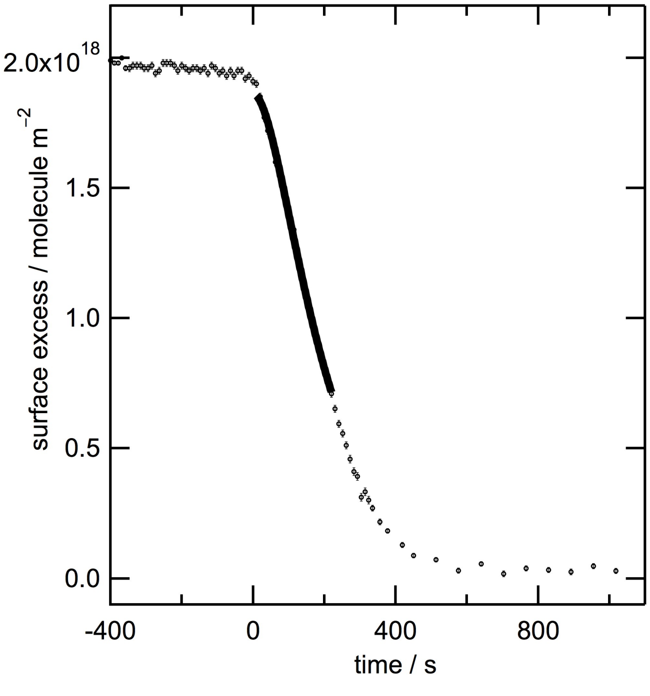

Figure S8. Surface excess of the ozonolysis of a monolayer of *d*-MO *vs*. time. *In situ* O_3-generation was initiated at $t = 0$. The solid line is a fit considering reactive decay and initial build-up of $[O_3]$ for $[O_3]_{in}$ = 100 ppb using fast-flow conditions to limit the effects of gas mixing (see run 8 in Table 1 of the main manuscript).

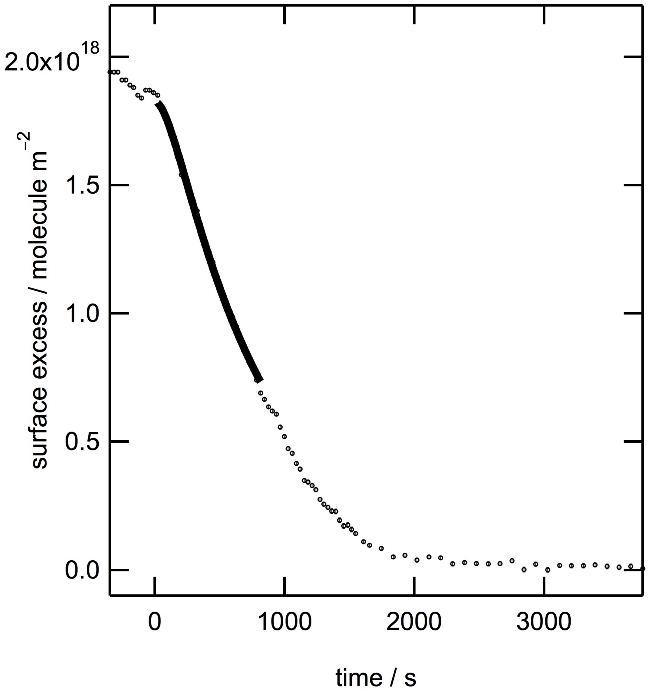

Figure S9. Surface excess of the ozonolysis of a monolayer of *d*-MO *vs*. time. *In situ* O_3-generation was initiated at $t = 0$. The solid line is a fit considering reactive decay and initial build-up of $[O_3]$ for $[O_3]_{in}$ = 22 ppb using fast-flow conditions to limit the effects of gas mixing (see run 4 in Table 1 of the main manuscript).

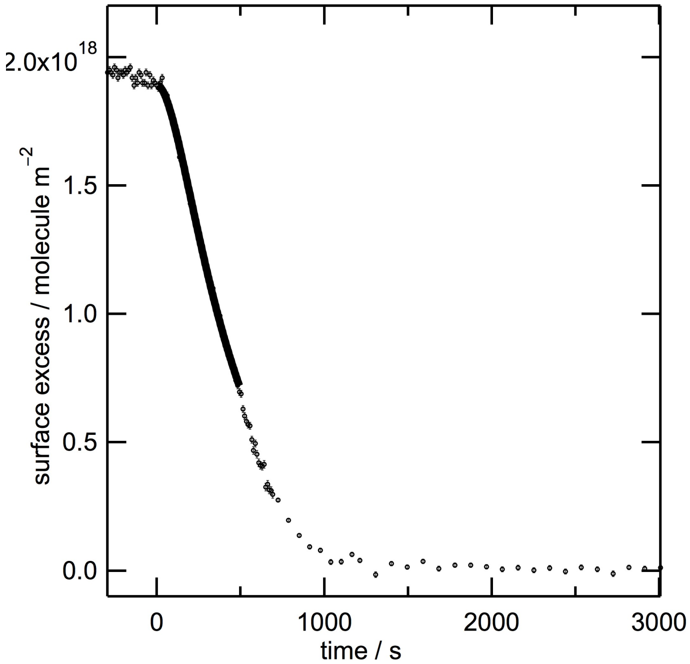

Figure S10. Surface excess of the ozonolysis of a monolayer of *d*-MO *vs*. time. *In situ* O_3-generation was initiated at $t = 0$. The solid line is a fit considering reactive decay and initial build-up of $[O_3]$ for $[O_3]_{in}$ = 51 ppb using fast-flow conditions to limit the effects of gas mixing (see run 6 in Table 1 of the main manuscript).

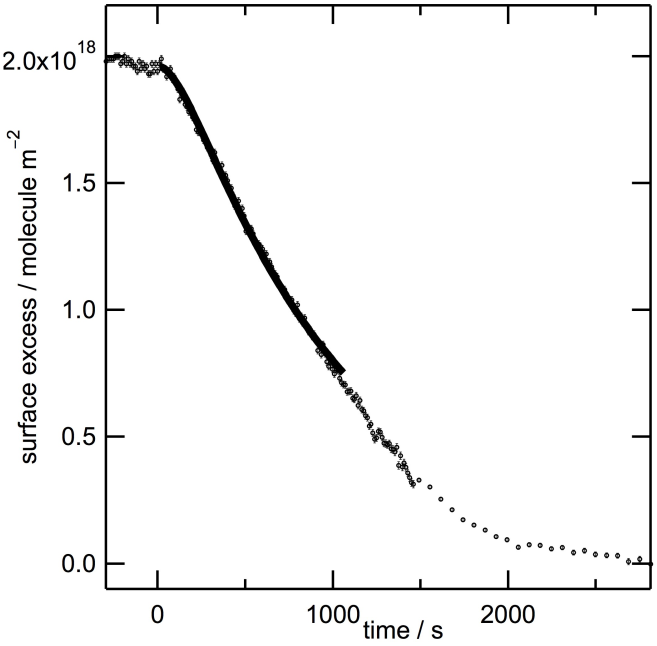

Figure S11. Surface excess of the ozonolysis of a monolayer of *d*-MO *vs*. time. *In situ* O_3-generation was initiated at $t = 0$. The solid line is a fit considering reactive decay and initial build-up of $[O_3]$ for $[O_3]_{in}$ = 17 ppb using fast-flow conditions to limit the effects of gas mixing (see run 3 in Table 1 of the main manuscript).

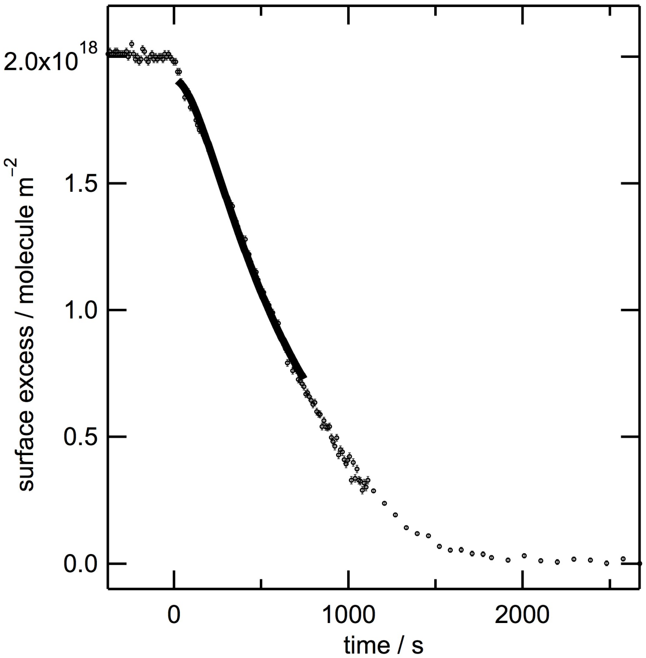

Figure S12. Surface excess of the ozonolysis of a monolayer of *d*-MO *vs*. time. *In situ* O_3-generation was initiated at $t = 0$. The solid line is a fit considering reactive decay and initial build-up of $[O_3]$ for $[O_3]_{in}$ = 40 ppb using fast-flow conditions to limit the effects of gas mixing (see run 5 in Table 1 of the main manuscript).

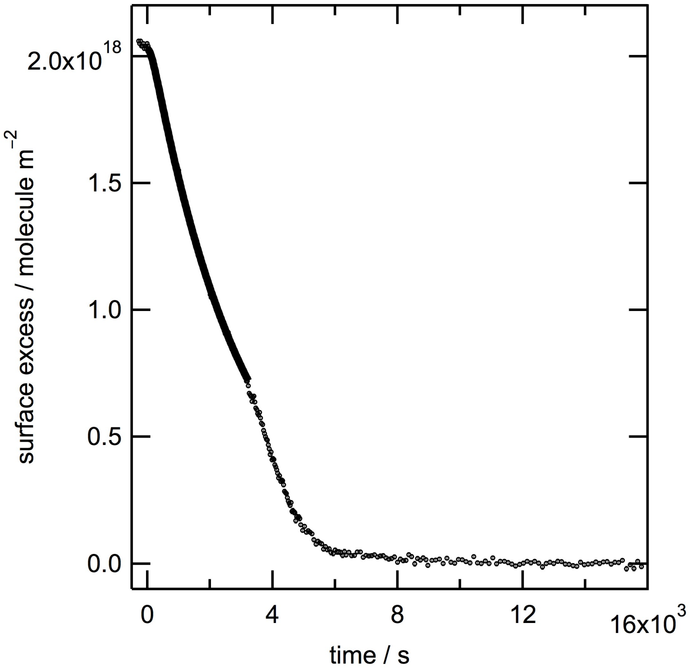

Figure S13. Surface excess of the ozonolysis of a monolayer of *d*-MO *vs*. time. *In situ* O_3-generation was initiated at *t* = 0. The solid line is a fit considering reactive decay and initial build-up of $[O_3]$ for $[O_3]_{in}$ = 9 ppb using fast-flow conditions to limit the effects of gas mixing (see run 2 in Table 1 of the main manuscript).

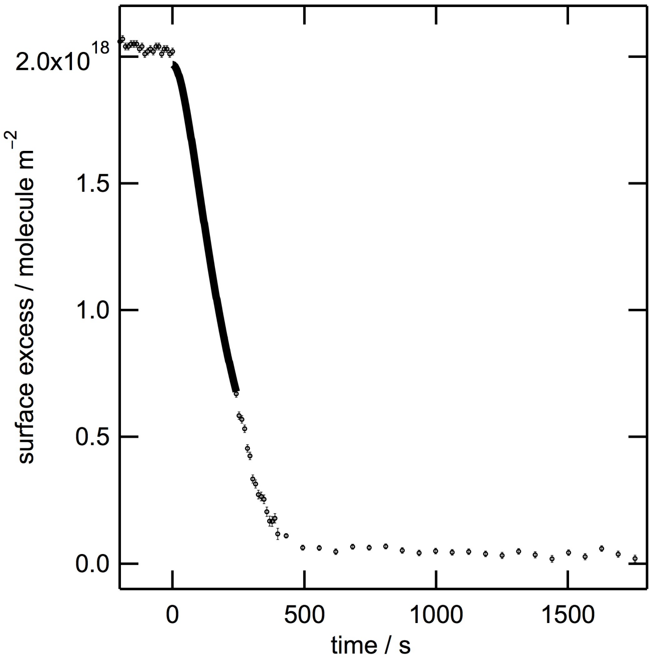

Figure S14. Surface excess of the ozonolysis of a monolayer of *d*-MO *vs*. time. *In situ* O_3-generation was initiated at *t* = 0. The solid line is a fit considering reactive decay and initial build-up of $[O_3]$ for $[O_3]_{in}$ = 100 ppb using fast-flow conditions to limit the effects of gas mixing (see run 9 in Table 1 of the main manuscript).

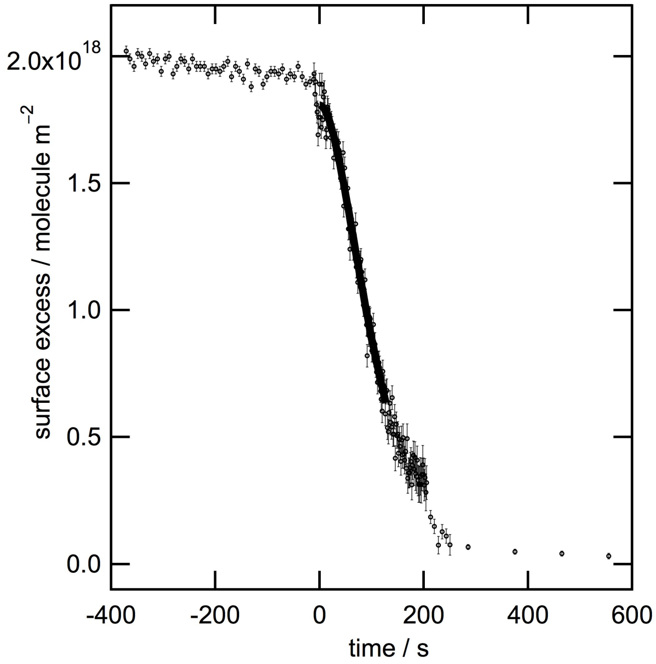

Figure S15. Surface excess of the ozonolysis of a monolayer of *d*-MO *vs*. time. *In situ* O_3-generation was initiated at $t = 0$. The solid line is a fit considering reactive decay and initial build-up of $[O_3]$ for $[O_3]_{in}$ = 227 ppb using fast-flow conditions to limit the effects of gas mixing (see run 11 in Table 1 of the main manuscript).

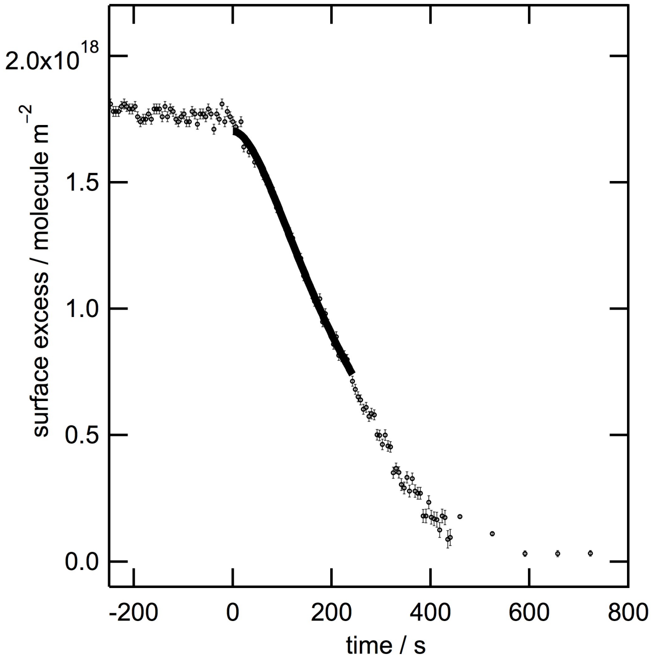

Figure S16. Surface excess of the ozonolysis of a monolayer of *d*-MO *vs*. time. *In situ* O_3-generation was initiated at $t = 0$. The solid line is a fit considering reactive decay and initial build-up of $[O_3]$ for $[O_3]_{in}$ = 75 ppb using fast-flow conditions to limit the effects of gas mixing (see run 7 in Table 1 of the main manuscript).

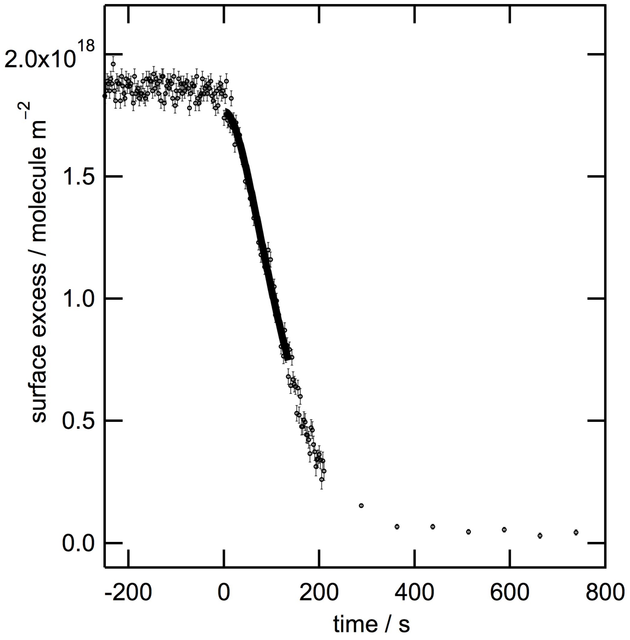

Figure S17. Surface excess of the ozonolysis of a monolayer of *d*-MO *vs*. time. *In situ* O_3-generation was initiated at $t = 0$. The solid line is a fit considering reactive decay and initial build-up of $[O_3]$ for $[O_3]_{in} = 167$ ppb using fast-flow conditions to limit the effects of gas mixing (see run 10 in Table 1 of the main manuscript).

C. Comparison of behaviour of oleic acid and its methyl ester at the air–water interface.

We measured isotherms for oleic acid and its methyl ester, methyl oleate at the air–water interface (Fig. S18 (a) and (b)) with three compression-expansion cycles for each monolayer. Methyl oleate exerts a higher surface pressure for a given area per molecule than oleic acid and collapses at lower surface pressures as demonstrated in the isotherms. Oleic acid levels off at 30 mN m^{-1} while methyl oleate plateaus already at 16 mN m^{-1} and there is a considerably higher loss of material for repeated compression-expansion cycles for methyl oleate. Above the surface pressure of 16 mN m^{-1} methyl oleate starts to form islands as illustrated in the Brewster Angle Microscopy image shown below (Fig. S19 (b)) contrasted to the isotropic behaviour at low surface pressures (Fig. S19 (a)).

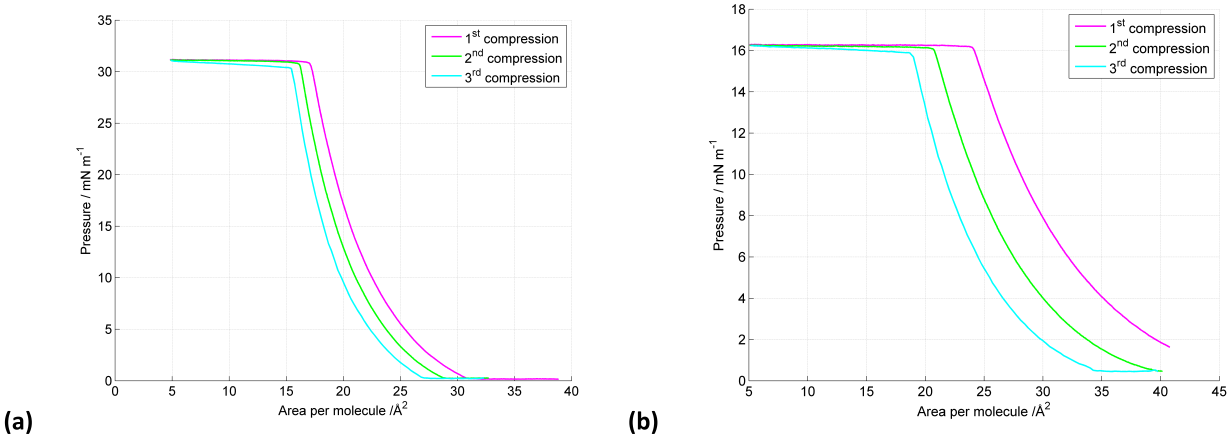

Figure S18. Isotherms measured for **(a)** oleic acid and **(b)** for its methyl ester, methyl oleate. Three compression-expansion cycles have been performed.

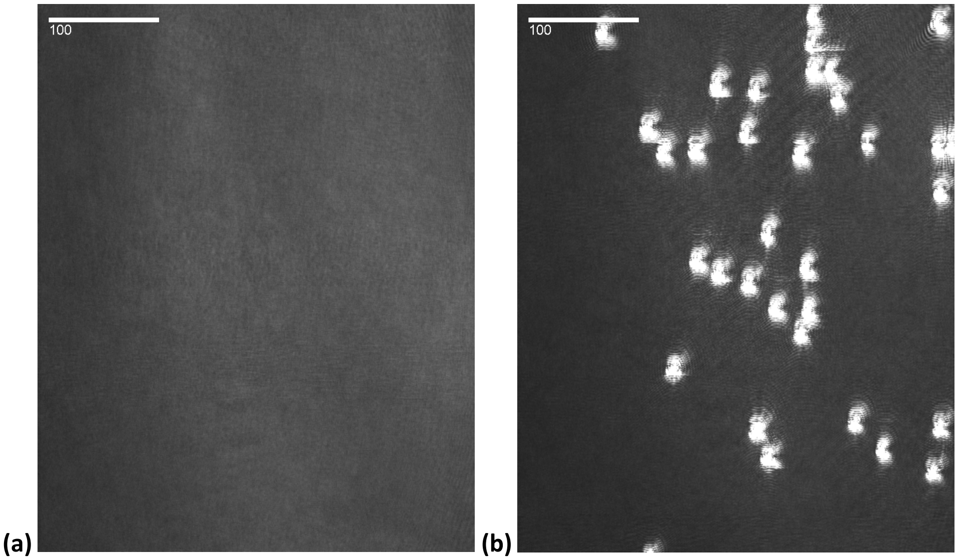

Figure S19. Brewster Angle Microscopy images for methyl oleate at **(a)** low surface pressure (the surface area covered is 676 cm^2) and **(b)** high surface pressure (the surface area was compressed to 90 cm^2). The white scale bars correspond to 100 μm.

D. Linear *versus* exponential fitting of the surface excess decays.

Fig. 1 in the main manuscript illustrates that the initial decay of the surface excess as a function of time shows an apparent linear trend. This apparent linear decay is consistent with our treatment of an exponential reactive decay convoluted with the initial build up of the ozone concentrations. Figs S20 (a) and (b) compare the expected decay behaviour for (a) instantaneous mixing (i.e. no gradient in the gas-phase oxidant concentration) and (b) considering the build up of ozone when entering the reaction chamber in our flow conditions. Linear fits are also displayed (red lines). It becomes apparent that (i) the simulated data displayed if Fig. S20 (b) look very similar to our experimentally observed decays and (ii) a linear fit works well for this decay unlike for the purely exponential decay in Fig. S20 (a). This apparent linear decay is an interesting coincidence, but a linear fit is not meaningful for longer reaction times since the surface excess levels off asymptotically towards zero (at least for highly pure surfactant samples). We thus consider the exponential fitting corrected for the build up of the gas-phase concentration of ozone to be the most suitable analytical approach.

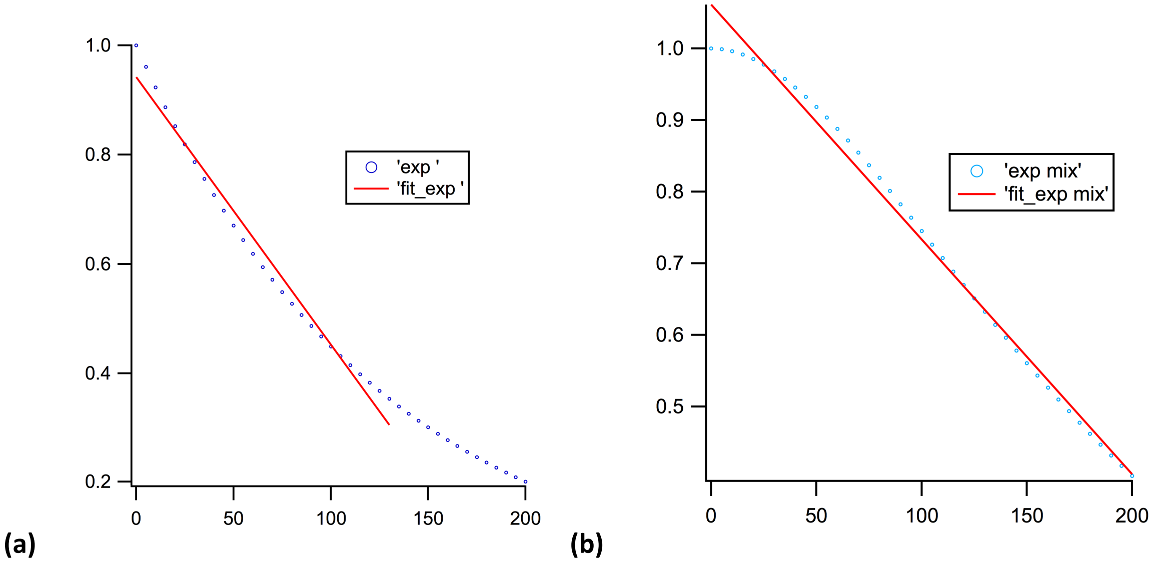

Figure S20. Simulated exponential decay of surface excess (arbitrary units) as a function of time for high ozone concentrations **(a)** without considering the build up of the gas-phase oxidant and **(b)** when considering the build up of the gas-phase oxidant. The red lines represent linear fits.

References

(1) LAMP, the Large Array Manipulation Program. http://www.ill.eu/data_treat/lamp/the-lamp-book/

(2) Fitter, J., Gutberlet, T. and Katsaras, J. Neutron Scattering in biology: techniques and applications, Springer, 2006

(3) Born, M. and Wolf, E. Principles of optics: electromagnetic theory of propagation, interference and diffraction of light, Pergamon Press, 7th Edition, 1999

(4) Nelson, A. Co-refinement of multiple-contrast neutron/X-ray reflectivity data using MOTOFIT. J. Appl. Cryst. 2006, 39, 273–276.